Materials Characterization 138 (2018) 154–164

Contents lists available at ScienceDirect

Materials Characterization

journal homepage: www.elsevier.com/locate/matchar

An integrated microstructural-nanomechanical-chemical approach to examine material-specific characteristics of cementitious interphase regions

Mahdieh Khedmati[a], Yong-Rak Kim[a,*], Joseph A. Turner[b], Hani Alanazi[a], Charles Nguyen[b]

[a] Department of Civil Engineering, 362 Whittier Research Center, University of Nebraska-Lincoln, United States
[b] Department of Mechanical and Materials Engineering, W342 Nebraska Hall, University of Nebraska-Lincoln, NE 68588, United States

ARTICLE INFO

Keywords:
Interfacial transition zone (ITZ)
Cementitious concrete, Geopolymer
Nanomechanical properties
Microstructure
Chemical mapping

ABSTRACT

Effective properties and structural performance of cementitious mixtures are substantially governed by the quality of the interphase region because it acts as a bridge transferring forces between aggregates and a binding matrix and is generally susceptible to damage. As alternative binding agents like alkali-activated precursors have obtained substantial attention in recent years, there is a growing need for fundamental knowledge to uncover interphase formation mechanisms. In this paper, two different types of binding materials, i.e., fly ash-based geopolymer and ordinary portland cement, were mixed with limestone aggregate to examine and compare the microstructures and nanomechanical properties of interphase region. To this end, microstructural characteristics using scanning microscopies, nanomechanical properties by nanoindentation tests, and spatial mapping of chemical contents based on the energy dispersive spectroscopy were integrated to identify and investigate the interphase region formed by the case-specific interactions between the matrix materials and limestone. The integrated microstructural-nanomechanical-chemical approach was effective to better understand links between material-specific properties of cementing phases. More specifically, the fly ash-based geopolymer paste was usually well bonded to the aggregate surface with a rich formation of N-A-S-H gel, while interfacial debonding was often observed between aggregate surface and paste in ordinary portland cement concrete. However, when a good bonding between aggregate and paste is formed, interphase region in PCC did not show any considerable difference in nanomechanical properties compared to the bulk paste.

1. Introduction

Cementitious materials are the backbone of the world's infrastructure, used in vast amounts to construct roads, buildings, bridges, and other structures. In cementitious mixtures, paste works as a glue that binds aggregate particles together and forms a strong whole. Effective properties and structural performance of the mixture are substantially dependent on the quality of the interphase region which exists between the aggregate and paste.

In conventional portland cement concrete (PCC), the interphase region is usually called Interfacial Transition Zone (ITZ) which is believed to act as a weak link between aggregate and paste and is susceptible to damage [1]. Due to the lower strength and stiffness of the interphase region, the first microcracks resulting from mechanical loads will appear in this region and will impact the overall mixture behavior [1–3]. Many studies, by using scanning electron microscopy (SEM), have identified the microstructural characteristics of the interphase region in concrete and shown that ITZ is extremely heterogeneous and distinct from the surrounding paste [2,4–8]. The higher porosity of the ITZ can significantly reduce the mechanical properties and durability of cementitious mixtures by allowing easier penetration of aggressive species into the mixtures [9]. Recently, nanoindentation which is a useful tool to derive the local nanomechanical properties of the materials, has been widely used to directly characterize the nanomechanical properties of the interphase region [10–16]. Although there are a lot of studies which have investigated the microstructure and mechanical properties of interphase region in PCC, studies on investigating chemical properties and integrating with mechanical and microstructural features of this region are limited. The adhesion between paste and aggregate particles has been characterized at the microscale by using particle probe scanning force microscopy [17,18] for different types of materials.

In addition to the weak ITZ, the high emission of carbon dioxide (CO_2) during the production of portland cement [19] is another drawback of the PCC mixtures. Recently, many studies have sought alternative pastes in concrete mixtures to reduce the CO_2 emission.

* Corresponding author.
E-mail addresses: mahdieh.khedmati@huskers.unl.edu (M. Khedmati), yong-rak.kim@unl.edu (Y.-R. Kim), jaturner@unl.edu (J.A. Turner), hani.alanazi@huskers.unl.edu (H. Alanazi), charlesnguyen@huskers.unl.edu (C. Nguyen).

https://doi.org/10.1016/j.matchar.2018.01.045
Received 10 October 2017; Received in revised form 18 January 2018; Accepted 30 January 2018
Available online 31 January 2018
1044-5803/

Geopolymer, which is an alkali-activated binder that can be obtained from industrial byproducts such as fly ash, has obtained particular attention in civil engineering as an alternative to portland cement due to its low emission of CO_2 without compromising mechanical properties [20–25]. In low calcium fly ash-based geopolymer material, sodium aluminosilicate hydrate (N-A-S-H) gel is the main reaction product and has similar elastic modulus to low density calcium silicate hydrate (C-S-H) which is the main reaction product in PCC [26–28]. In spite of an increasing attention towards the use of geopolymer concrete (GPC) as an alternative cementitious mixture, few studies have investigated the interphase between the geopolymer paste and aggregates [29,30].

2. Research Objective and Scope

The primary objective of this study is to investigate the microstructural, nanomechanical, and chemical characteristics of the interphase region in cementitious mixtures with two representative binding agents: fly ash-based geopolymer and portland cement. For this purpose, three different aspects of investigation; geometrical, mechanical, and chemical; were integrated. Geometrically, scanning electron microscopy (SEM) and laser scanning microscopy (LSM) were used to examine the microstructure of the interphase region. Mechanically, nanoindentation tests were conducted to evaluate the nanomechanical response of the material. Chemically, energy dispersive spectroscopy (EDS) was used to obtain information about the influence of the material chemical composition on the formation of the bond between aggregate and paste in the interphase region.

3. Materials and Laboratory Tests

3.1. Materials and Mixture Ratios

Class F fly ash, whose chemical composition is given in Table 1, was used in this study as an aluminosilicate source material for making geopolymer concrete. Class F fly ash obtained from Boral, Colorado was produced from the combustion of pulverized bituminous or Texas lignite coal. The specific gravity of the fly ash is 2.37. The alkaline activator solution was a mixture of sodium hydroxide and sodium silicate solutions. Sodium hydroxide solution of 12 M concentration was prepared by dissolving sodium hydroxide pellets with a purity of 98% in distilled water. Sodium silicate solution (28% SiO_2, 9% Na_2O, and 63% water) was chosen for this study. The mass ratio of sodium silicate to sodium hydroxide solutions was kept 1.0. Ordinary portland cement Type I, with the chemical compositions shown in Table 1, was used to produce the conventional concrete for comparison. Crushed limestone with a maximum aggregate size of 19 mm was used for mixing with each binding material.

The GPC and PCC samples were prepared with the same amount of binder and aggregate. Geopolymer specimens were prepared with an alkali solution to fly ash ratio of 0.4, and PCC specimens were prepared with water to cement (w/c) of 0.4. The fly ash and local crushed limestone were dry-mixed for 3 min, and then the alkaline solution was added and mixed for another 5 min. The GPC and PCC specimens were cast in 100 mm by 200 mm concrete cylinder molds. The GPC specimens were covered and cured at 60 °C for 24 h in a laboratory oven, then demolded and stored in a controlled temperature of 23 ± 2 °C. PCC specimens had different curing regimes where specimens after casting were sealed using lids and plastic bags to prevent excessive moisture loss. After 24 h, PCC specimens were demolded and placed in water for 28 days.

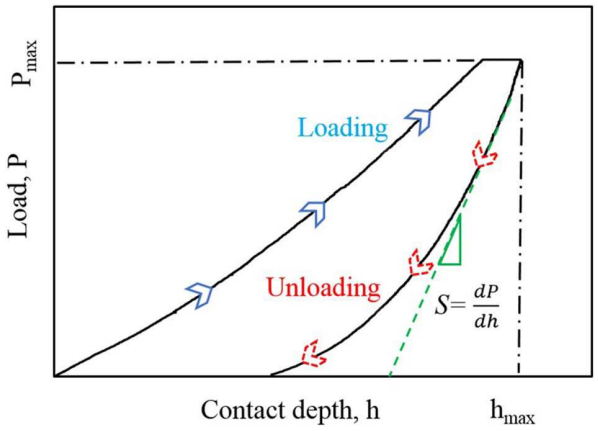

Fig. 1. Schematic of load–displacement curve from nanoindentation.

3.2. Specimen Preparation

Since analysis of nanoindentation experiments assume that the indentation occurs on a flat surface, smoothening the surface and reducing the roughness to a tolerable level is critical for receiving accurate results [31]. Therefore, once each mixture was fully cured, the center part of the mixture specimen was extracted and then each piece was cut with MTI digital low speed diamond saw into small slices of approximately 10 mm × 10 mm cross section and 4-mm thickness. Before grinding and polishing, which are necessary to achieve a flat surface, samples were vacuum impregnated with a low viscosity epoxy resin. Epoxy fills the pores of the sample and when it gets hardened, it maintains the microstructure unchanged and enables it to tolerate the stresses induced from grinding and polishing procedure without alteration [32]. After epoxy impregnation, silicon carbide abrasive papers of 400, 600, 800, and 1200 grit were used to remove material by grinding. After grinding with the 1200 grit paper, for removing the scratches resulted from sawing and grinding, the surface was polished using a sequence of successively finer alumina suspension particles (1 μm, 0.3 μm, and 0.05 μm). Finally, the samples were cleaned in an ultrasonic bath in ethanol to remove all foreign particles that remained from the polishing process.

3.3. Laser Scanning Microscopy (LSM)

Laser Scanning Microscopy (LSM) is a type of optical microscopy which uses a focused beam of a laser that can scan the sample and reflect intensity that is displayed as a function of position. A digital reflected light image of the sample can be created as a result. LSMs are able to collect both an optical image and high-resolution surface data by combining white light with a laser light source. Since the resolution is determined by the position of the beam rather than the pixel size of the detector, nanometer-level resolution digital images of any material can be generated by using LSM. By analyzing the intensity of the returned laser light relative to the z-position of the laser, nanometer-level

Table 1
Chemical composition of materials (%).

Component	SiO_2	Al_2O_3	Fe_2O_3	CaO	MgO	K_2O	SO_3	Na_2O	Na_2O_3	L.O.I.*
Class F fly ash	51.82	23.07	13.02	2.79	0.85	2.52	1.23	0.71	–	2.41
Portland cement Type I	20.99	6.19	3.86	65.96	0.22	0.6	0.55	–	0.17	1.46

* L.O.I. loss on ignition.

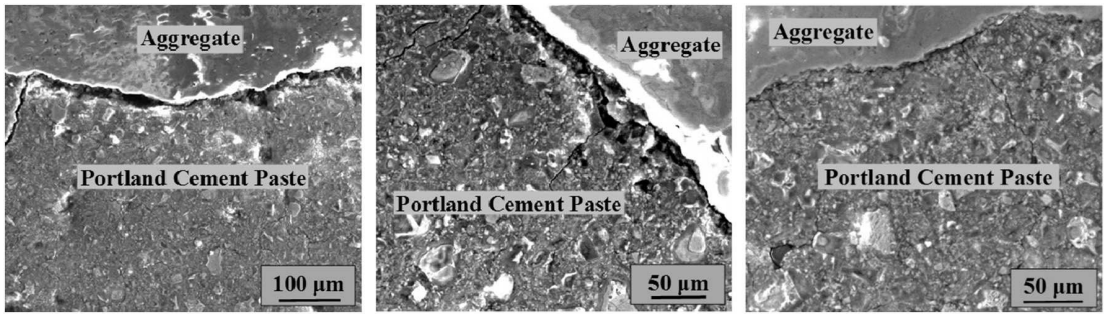

Fig. 2. SEM images of interphases in PCC.

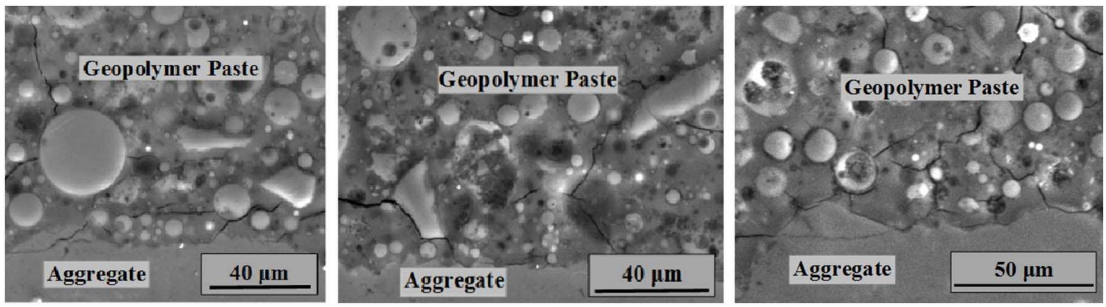

Fig. 3. SEM images of interphases in GPC.

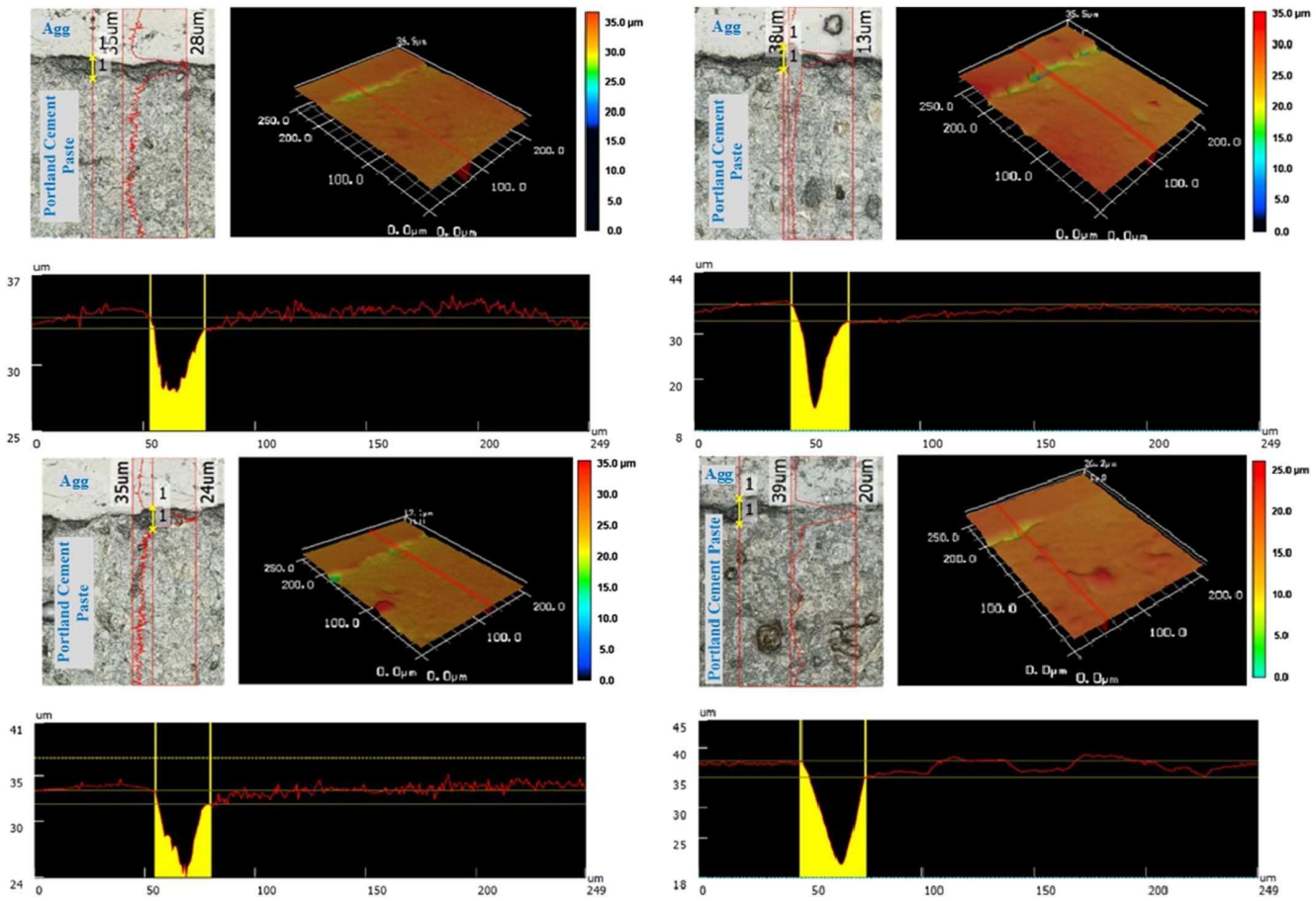

Fig. 4. Topography LSM images across aggregate-paste in PCC.

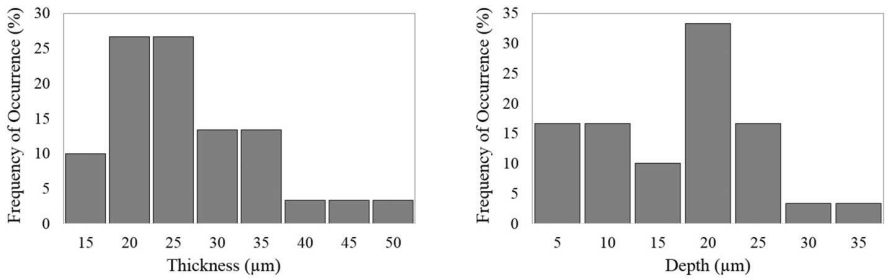

Fig. 5. Frequency distribution of thickness and depth of interfacial debonding.

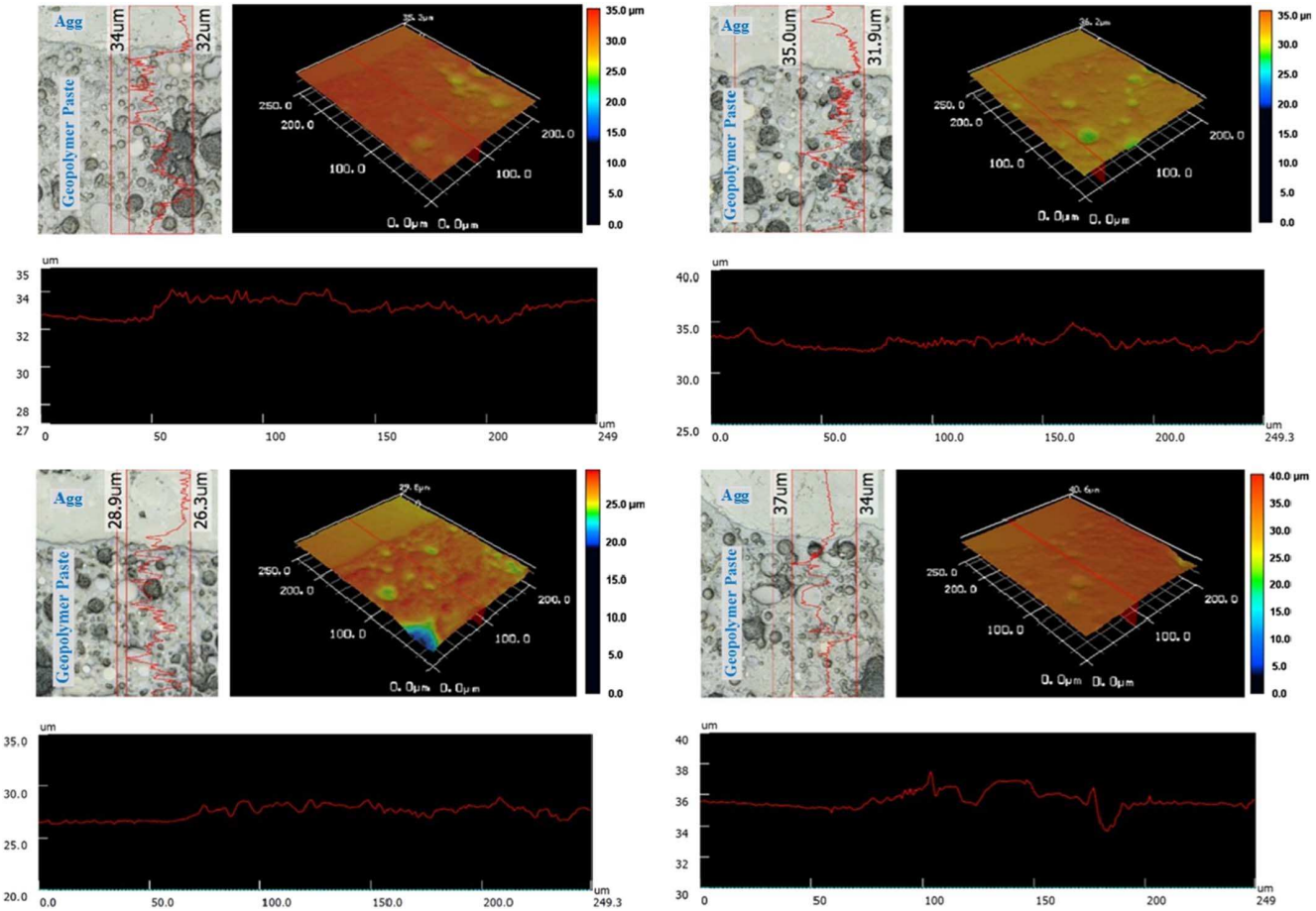

Fig. 6. Topography LSM images of aggregate-paste in GPC.

heights can also be measured, and surface topography can be provided at any selected specimen micro areas [33–36].

3.4. Scanning Electron Microscopy - Energy Dispersive Spectroscopy (SEM-EDS)

A scanning electron microscope (SEM) in high-vacuum mode was used on the impregnated and polished surface of the mixture samples to acquire microscale images and provide microstructural characterization of the samples. SEM is a powerful tool that can provide micro- and nano-scale images by using a focused beam of electrons. SEM images can reveal levels of details and complexity that are not achievable by conventional optical microscopes.

The chemical composition of the reaction product of the mixtures can be determined by using the energy dispersive X-ray spectroscopy (EDS) detector installed on the SEM. In this study, EDS analysis in conjunction with SEM imaging was performed to produce the elemental mapping of the interphase region. In addition, SEM-EDS line scans were employed to measure the elemental concentration across the aggregate-paste. A thin coating of carbon was applied on the surface of specimens before conducting SEM imaging and EDS mapping. The carbon coating serves to dissipate excessive charge from the specimen without affecting the image contrast or interfering with elements of interest [32,37].

3.5. Nanoindentation Testing

To determine the nanomechanical properties across the interphase region of each specimen, a nanoindentor instrument with a pyramid shaped diamond Berkovich tip was used. To eliminate the effects of sample roughness on the accuracy of the results, the indentation depth should be larger than the root mean square (RMS) roughness. Since the

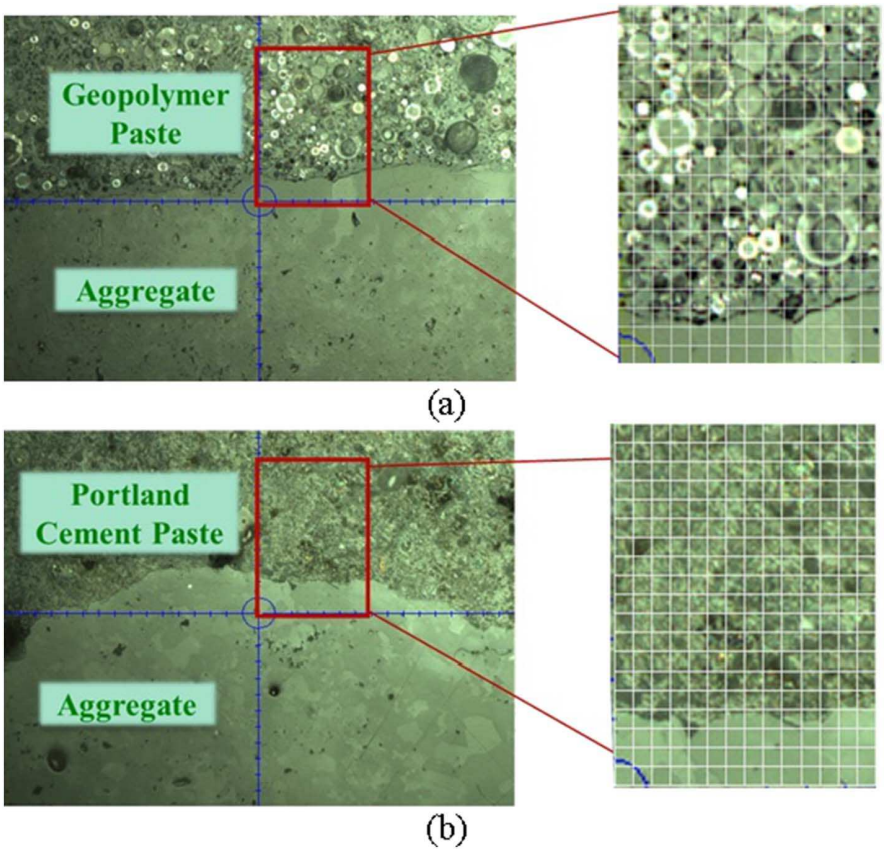

Fig. 7. Optical Microscopy image of the indented areas with a dimension of 190 μm × 140 μm in (a) GPC, and (b) PCC.

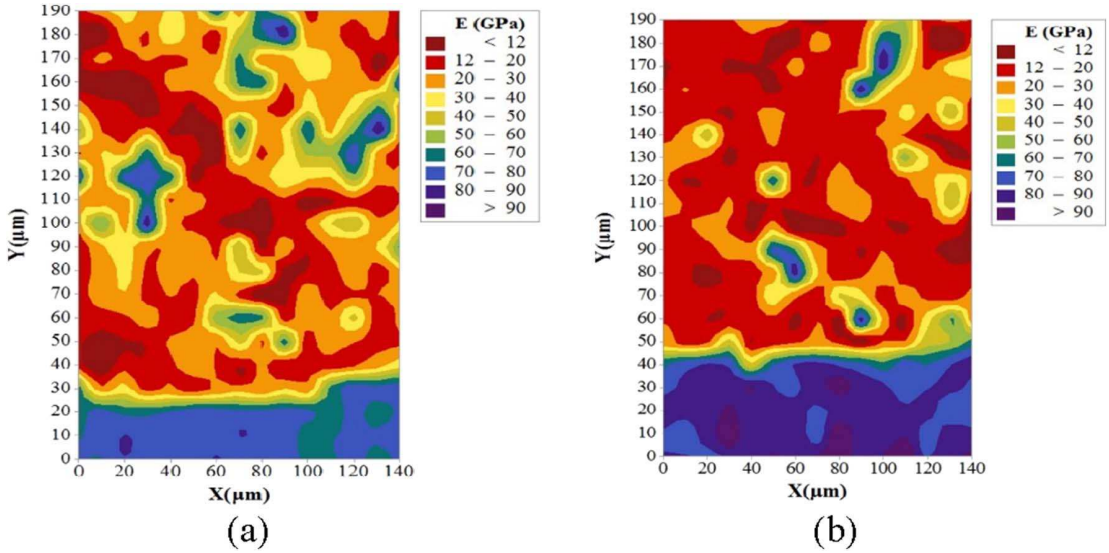

Fig. 8. Contour maps of elastic modulus (GPa), (a) GPC, (b) PCC.

average measured RMS roughness in multiple areas of both GPC and PCC is around 80 nm, an average penetration depth of 300 nm which is around 3–4 times larger than the surface roughness of samples should be satisfactory to avoid effects of roughness [38].

A trapezoidal quasi-static load-control mode of loading was applied on the polished samples with a peak load of 2000 μN. The loading and unloading part of this load function had a constant rate of 200 μN/s. The peak load was kept constant for 5 s to eliminate the effects of any possible creep [39]. A schematic load vs. displacement curve which is a typical response of materials under applied load in nanoindentation test is illustrated in Fig. 1.

The indentation modulus or reduced modulus (E_r) is obtained as defined by:

$$E_r = \frac{1}{\beta}.\frac{S}{2}.\frac{\sqrt{\pi}}{\sqrt{A_c}} \quad (1)$$

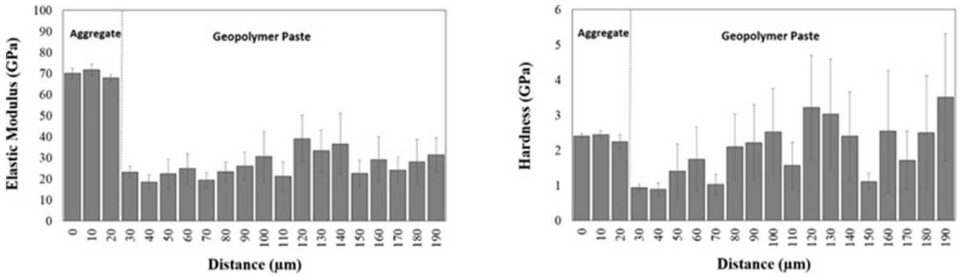

Fig. 9. Grid indentation modulus and hardness across aggregate-paste in GPC.

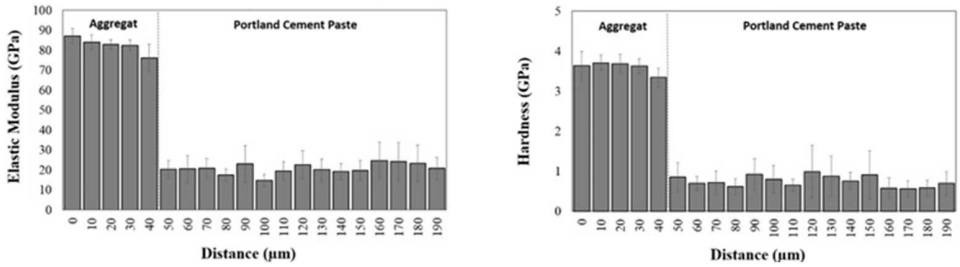

Fig. 10. Grid indentation modulus and hardness across aggregate-paste in PCC.

In Eq. (1), β is a dimensionless correction factor that accounts for the shape of the indenter tip and takes a value of 1.081 for Berkovich tips [40], $S = dp/dh$ is the slope of the unloading part of the load vs. displacement curve, and A_c is the projected contact area, which can be extrapolated from the indentation depth h using the Oliver and Pharr method [41]. The elastic deformation effect of the indenter is assumed known such that the absolute elastic modulus (E_s) that is solely responsible for the indentation depth recovery during the unloading process can be determined. This relation is given as:

$$\frac{1}{E_r} = \frac{1-\nu_s^2}{E_s} + \frac{1-\nu_i^2}{E_i} \tag{2}$$

where E and ν are the Young's modulus and Poisson's ratio, respectively; here the subscripts correspond to the specimen (s) and diamond indenter tip (i) elastic properties. The elastic modulus and the Poisson's ratio of the diamond indenter are equal to 1140 GPa and 0.07, respectively.

The hardness of the material can also be obtained from:

$$H = \frac{P_{max}}{A_c} \tag{3}$$

where P_{max} is the peak load at the maximum of the curve.

4. Results and Discussion

4.1. Microstructural Imaging

SEM images of a typical microstructure at the interphase regions of PCC and GPC samples are shown in Fig. 2 and Fig. 3, respectively. The SEM images were taken from multiple locations around the aggregates in both samples. It was observed that in some locations in the PCC sample, a clear interfacial debonding with high porosity exists between aggregate and paste.

The interphase between aggregate and paste in GPC was substantially different than that of the PCC. It was generally observed that geopolymer paste was tightly bonded to the surface of the aggregate in almost every interphase region in this sample.

In conjunction with SEM imaging, LSM topography images were taken from randomly selected locations on the interphase regions of both samples. Fig. 4 shows three-dimensional views and profiles of the PCC sample across some aggregate-paste regions. The profiles can detect and quantify depth and thickness of specific regions where interfacial debonding occurred. The depth and the thickness of the interfacial debondings in 30 different locations on the sample were captured, and results are depicted in Fig. 5 in a form of histogram. As can be seen, the thickness and depth of interfacial debonding vary in different locations of the sample and are in a range of 15–50 μm and 5–35 μm, respectively, which agrees well with other similar studies [42–45] indicating that the thickness of ITZ in PCC is around 20–50 μm.

Fig. 6 shows representative three-dimensional LSM images of the GPC sample. It was observed that the variation of elevation from aggregate to paste was much less than PCC. In contrast to PCC, there was no significant gap or separation detected in the interphase region.

4.2. Nanomechanical Characterization

In this study, nanoindentation tests were conducted on areas selected on the interphase region around aggregates on both GPC and PCC. The indented areas had the dimension of 190 μm × 140 μm and 300 indents were performed in each studied area. The distance between the indents in both vertical and horizontal directions were 10 μm to avoid the effects of adjacent imprints. The grid areas of the nanoindentation tests of both samples are shown in Fig. 7(a) (GPC) and Fig. 7(b) (PCC).

As mentioned in the previous subsection (i.e., microstructural imaging), in some areas of the PCC sample, the interphase region appeared weak with high porosity (or boundary separation) existing between aggregate surface and paste. The high porosity interphase region in PCC is not desired for nanoindentation testing that requires very smooth surface for accurate measurement. For this reason, the interphase regions of PCC with high porosity (or significant boundary separation) were avoided intentionally, and the indented area was selected on a zone which appeared dense.

Fig. 8 shows the resulting contour maps of the elastic modulus of both mixtures. A more heterogeneous distribution of elastic moduli appeared in GPC than PCC. The dark red areas have the lowest moduli (less than 12 GPa) which are considered attributing to weak zones. The results show that local weak zones are placed in the entire indented areas on both samples. There was no clear weak interphase observed for either case, which indicates that interphase properties are not

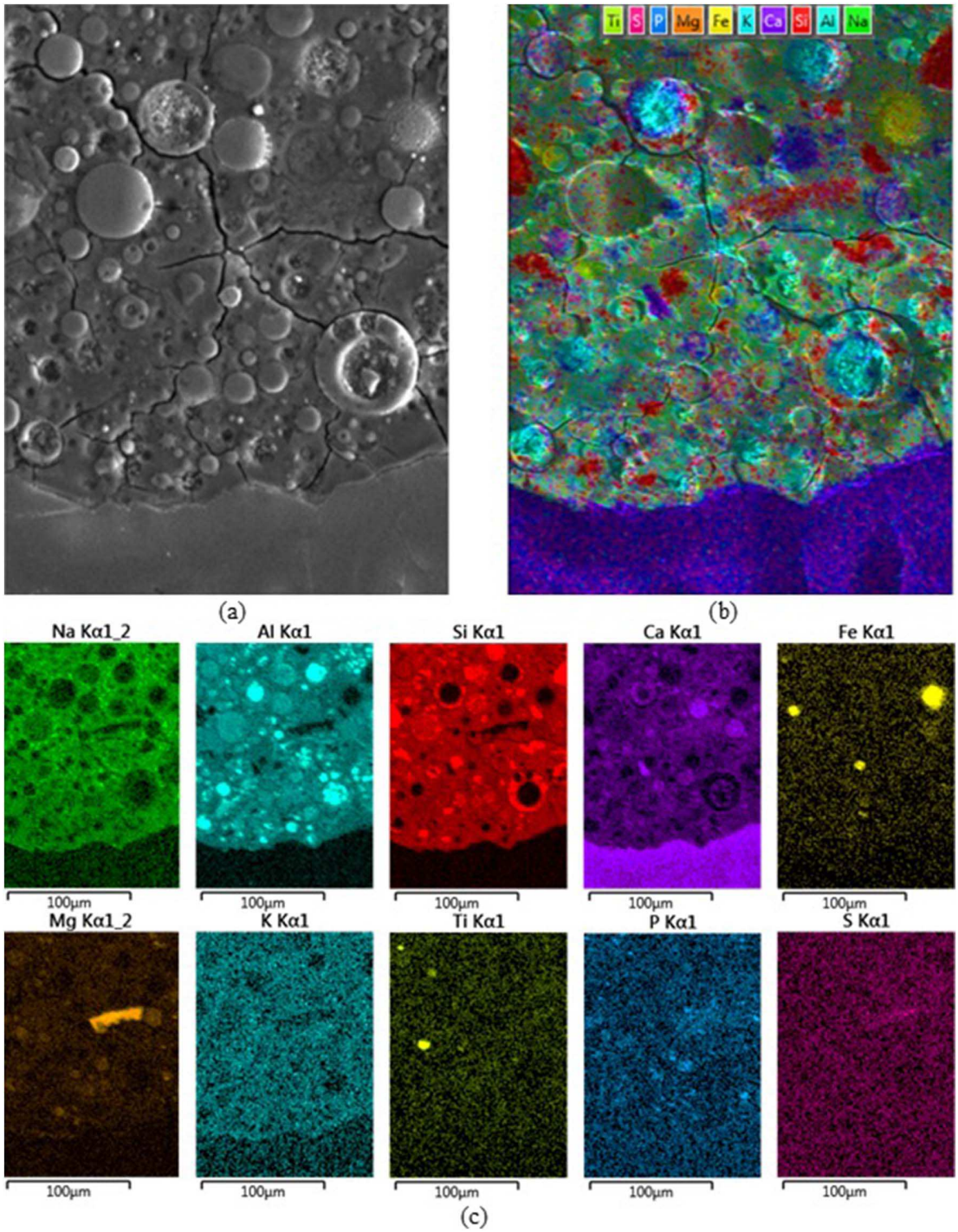

Fig. 11. Qualitative EDS map analysis of GPC mixture, (a) SEM image, (b) overlay map, (c) individual elemental maps.

compromised when the paste is tightly bonded to the surface of the aggregate.

Fig. 9 and Fig. 10 show the distribution of elastic modulus and hardness versus distance across the aggregate-paste of GPC sample (Fig. 9) and PCC sample (Fig. 10), respectively. Clearly, there was a big difference in elastic properties between limestone aggregate and both cementitious matrix phases. Fig. 9 showed more heterogeneous nature of the geopolymer paste which resulted in a larger variation of elastic modulus and hardness. In contrast to GPC, the variation of mechanical properties across the aggregate-paste in PCC was somewhat smaller. No considerable variation of nanomechanical properties within entire cement paste was observed in Fig. 10. The uniformity of the elastic modulus and hardness across aggregate-paste in PCC is also dependent on the sample locations since calcium hydroxide crystals may exist in the porous regions between aggregates and cement paste.

Many studies define the existence and dimension of the ITZ in cementitious mixtures as the distance between the aggregate and paste where the values of the elastic modulus and hardness are unstable and there is a great variation in the values between studies [11,13,38]. However, identifying the ITZ and determining the dimension by just

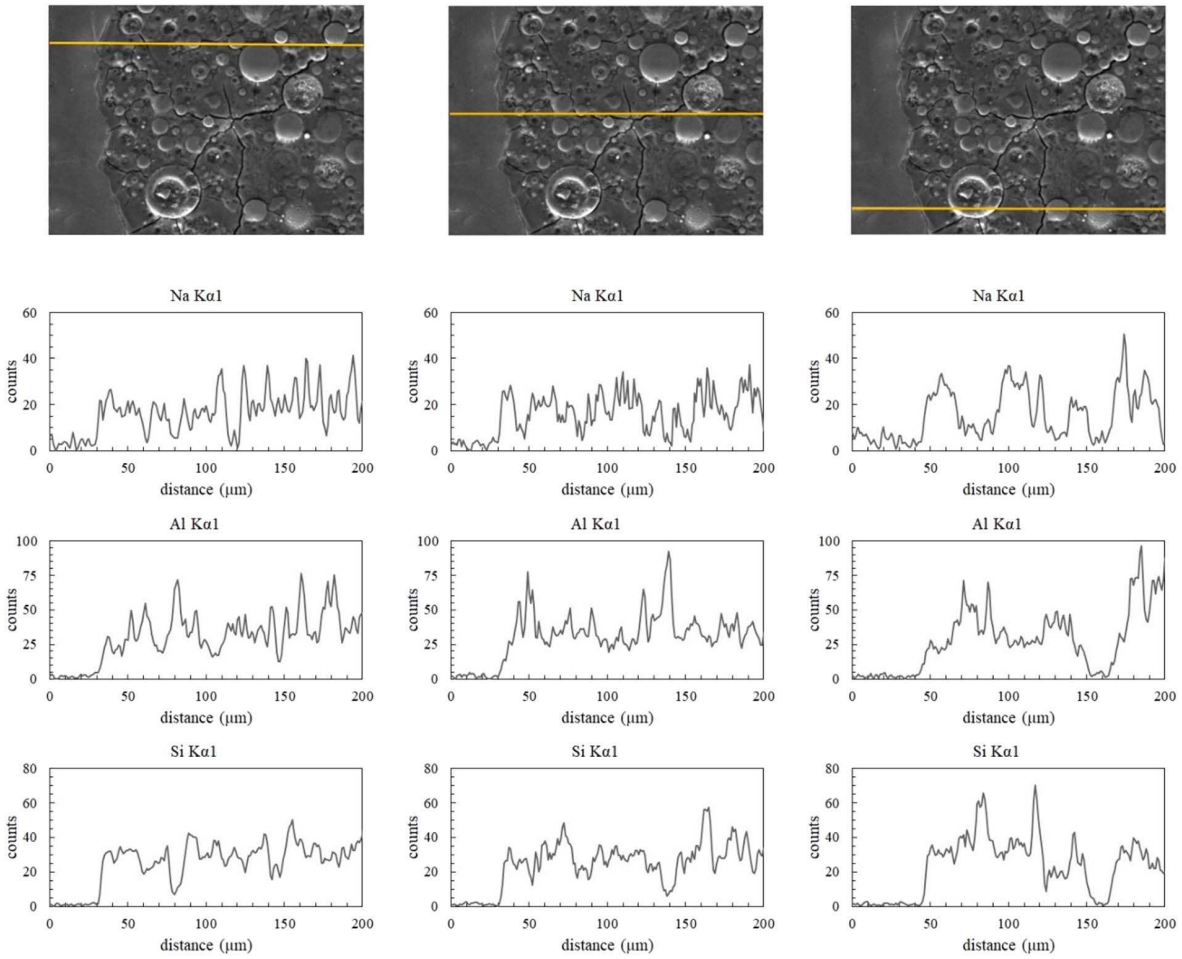

Fig. 12. SEM-EDX line scan across aggregate-paste in GPC.

defining the unstable area from the nanomechanical test results may not be an accurate way due to the possible mismatching between mechanical properties and actual phases that are usually highly heterogeneous. For this reason, identifying the ITZ with aids of other methods such as chemical (elemental) analysis can be attempted. The EDS analysis in conjunction with SEM imaging can produce the elemental (chemical) mapping of the target region as illustrated in the next subsection.

4.3. EDS Analysis

The distribution of chemical elements in reaction compounds was studied by utilization of elemental mapping by SEM-EDS. Fig. 11 shows the SEM micrograph, overlay map of the GPC on the same area that was studied in the previous section, and distribution of individual chemical elements. The brightest regions of the elemental maps indicate the highest concentrations of the chemical element analyzed. The overlay map represents the combination of all elemental maps.

The aggregate area is shown in purple which shows the high concentration of Ca on limestone ($CaCO_3$). It can be seen that the region around the limestone aggregate has a high Na, Al, and Si content which seems an indication of the N-A-S-H gel existence in this region. More information about the aggregate-paste interphase can be obtained from the EDS line scans by mainly focusing on the distribution of elements present in the highest concentrations in the paste.

The line scan results of the main reaction products (Na, Al, and Si) of the geopolymer are shown in Fig. 12. Each graph shows the distribution of each element across the interphase (from the edge of limestone aggregate to the edge of geopolymer paste). Apparently, the concentration of Na, Al, and Si elements is close to zero on the limestone whereas there is an abrupt increase in all elements at the limestone-paste boundary region which is identified by matching the SEM image with the results of the line scan.

Based on the chemical composition of raw fly ash (shown in Table 1) where only a small amount of Na (0.71%) is present, Fig. 12 implies that the abrupt increase in concentration of Na at the paste side of the interphase might be an indication of formation of N-A-S-H gel, because the alkali activated paste will become rich in Na after mixing fly ash with alkaline activator solution which was a mixture of sodium hydroxide (NaOH) and sodium silicate (Na_2OSiO_2) solutions. The high concentration of Al and Si elements are also observed in the region. These observations can lead to an interpretation of the existence of N-A-S-H (Sodium, Alumina, Silicate, Hydrate) gel in the interphase region that can form a strong bond between aggregate and paste. This chemical analysis can then be integrated with the nanomechanical property results and microstructural observation. In Fig. 9, the GPC depicts ~20 μm region around the aggregate with an average elastic modulus around 18 GPa and average hardness around 0.9 GPa which could be attributed to the mechanical properties of the main geopolymerization product, N-A-S-H gel [27,28]. As a result, the existence of the N-A-S-H gel in the vicinity of the aggregate can lead to a dense interphase region as demonstrated in Fig. 3 and Fig. 6.

The SEM image, the overlay map of the PCC, and the distribution of individual chemical elements on the same area that was studied in the previous section is presented in Fig. 13. One well-accepted finding is that ITZ in PCC consists of a higher amount of calcium hydroxide (C-H)

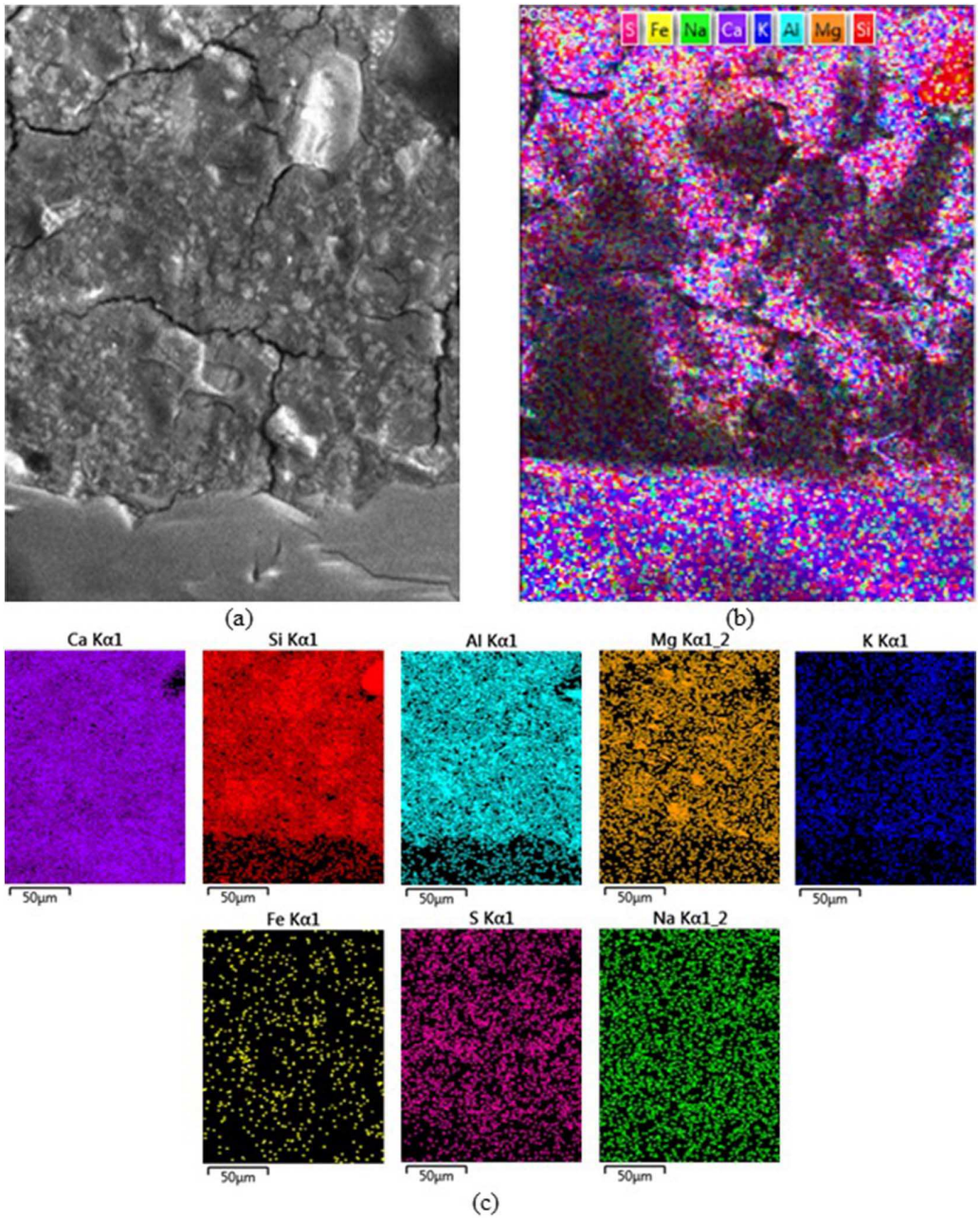

Fig. 13. Qualitative EDS map analysis of PCC mixture, (a) SEM image, (b) overlay map, (c) individual elemental maps.

and less formation of C-S-H, which may compromise mechanical properties of the PCC ITZ. The EDS results in this study showed that the Ca and Si are relatively well distributed in the entire paste region including the vicinity of limestone. The coexistence of these two elements around the aggregate indicates the existence of C-S-H, the main reaction product from PCC hydration.

The distribution of Ca and Si was also examined by line scans as depicted in Fig. 14. It shows that Ca is well distributed from aggregate to paste, while Si appeared from the boundary of limestone aggregate and became more apparent in the paste region by exhibiting a transition in the vicinity of aggregate, which clearly indicates the formation/creation of C-S-H within the interphase region. In general, EDS results agree well with the nanomechanical test results presented in Fig. 8 and Fig. 10. Mechanical properties of the interphase region in PCC were not very different from properties of cement paste far away from the aggregate surface when a good bonding between aggregate and paste is formed. This would be due to rich formation of C-S-H which enables the good bonding. However, as demonstrated in Fig. 4 and Fig. 5, ITZ of PCC often exhibits weak zones of high porosity (and/or boundary separation) in the vicinity of aggregates, which supports the general observation that implies diminished mechanical properties of the PCC ITZ [4,46].

5. Concluding Remarks

This paper provided a coupled microstructural, nanomechanical, and chemical study on interphase region between limestone particle and the surrounding cementitious paste. Two types of matrices: ordinary portland cement paste and geopolymer paste, were used and compared in this study.

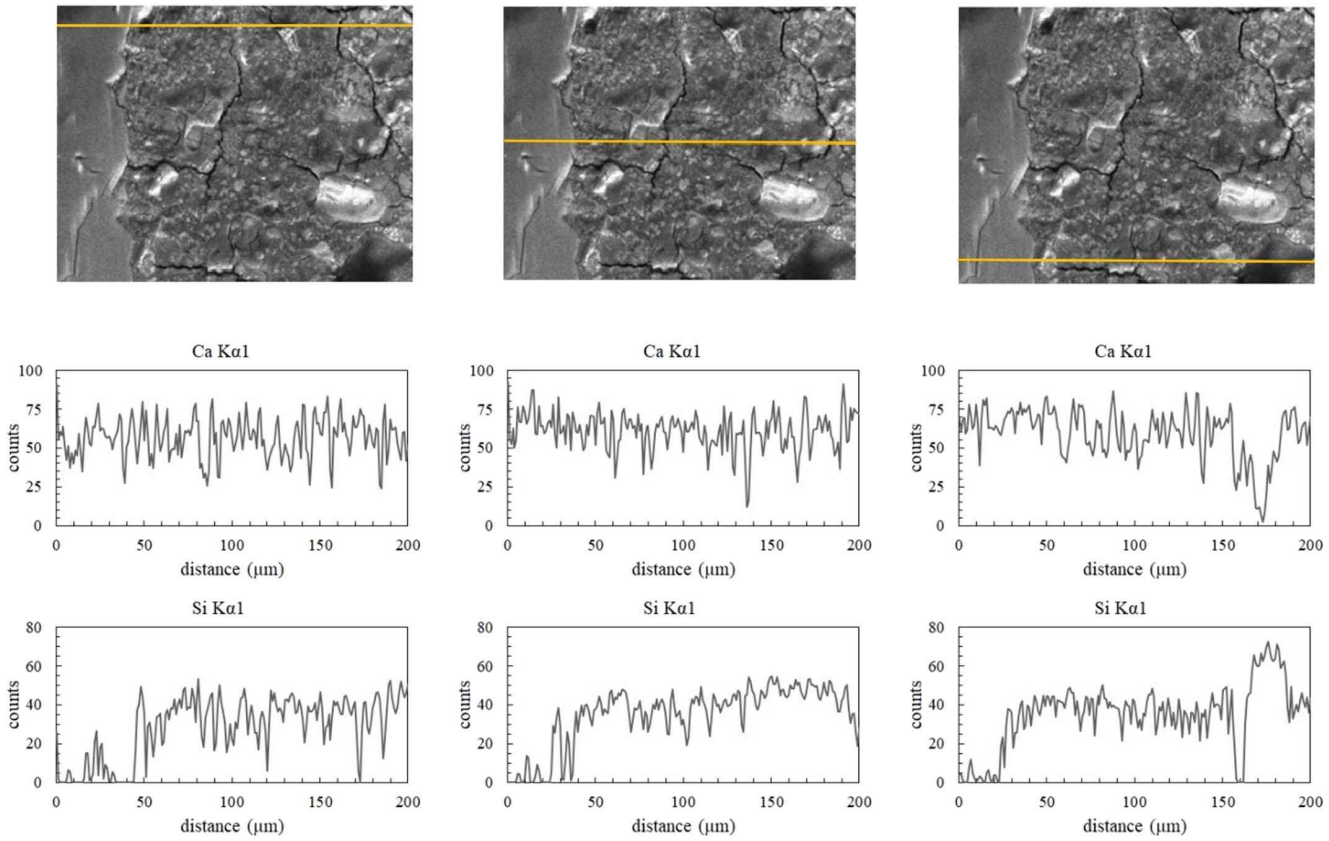

Fig. 14. SEM-EDX line scan across aggregate-paste in PCC.

The microstructural characterization of the interphase region was analyzed by SEM and LSM. The SEM images taken from multiple locations around the aggregates showed that in some locations in the PCC sample, a clear interfacial debonding exists between aggregate and paste, while geopolymer paste was usually well bonded to the aggregate surface in almost every interphase region in the sample. The three-dimensional topography image across the aggregate-paste which was analyzed by using LSM showed that the thickness and depth of the interfacial debonding in PCC are up to 50 μm and 35 μm, respectively. This study also presented nanomechanical properties across aggregate-paste. The interphase in PCC did not show any considerable difference in nanomechanical values compared to the bulk paste when a good bonding between aggregate and paste is formed. In GPC, a more heterogeneous distribution of elastic moduli appeared than PCC, which seems due to creation of multiple phases (such as N-A-S-H gel, fly ash grains in different reaction levels, pores, shrinkage cracks, etc.). The EDS chemical analysis supported the nanomechanical findings and showed the existence of N-A-S-H gel in the interphase areas of the GPC sample. A narrow band around 20 μm thick in the vicinity of aggregate where the average elastic modulus was about 18 GPa might correspond to the formation of N-A-S-H. In PCC, Ca was well distributed from aggregate to paste, and Si appeared from the boundary of limestone aggregate and became more apparent in the paste region by exhibiting a transition in the vicinity of aggregate. Chemical mapping results were in good agreement with the nanomechanical and microstructural results.

This study demonstrates that the method integrating microstructure examination, nanomechanical property characterization, and spatial mapping of chemical elements can help identify the small region such as interphase region that is formed through the case-specific interactions between the matrix materials and aggregates. However, findings from this study need further investigation to make more definite conclusions. Smaller-scale analysis, such as the atomic force microscopy (AFM) integrated with a chemical composition analysis to better identify and characterize individual phases, would be more informative. This is currently under investigation by the authors.

Acknowledgements

The authors are grateful for the financial support received from the National Science Foundation (Grant No. CMMI-1635055). We also like to acknowledge testing facilities: the Nano-Engineering Research Core Facility (NERCF) and the Nebraska Center of Materials and Nanoscience (NCMN) at the University of Nebraska-Lincoln to conduct the laboratory tests for this study.

References

[1] K.L. Scrivener, P.L. Pratt, Characterization of Interfacial Microstructure. Interfacial Transition Zone in Concrete, 2 (1996), pp. 3–18.
[2] T. Akçaoğlu, et al., Assessing the ITZ microcracking via scanning electron microscope and its effect on the failure behavior of concrete, Cem. Concr. Res. 35 (2) (2005) 358–363.
[3] S. Erdem, et al., Influence of the micro-and nanoscale local mechanical properties of the interfacial transition zone on impact behavior of concrete made with different aggregates, Cem. Concr. Res. 42 (2) (2012) 447–458.
[4] S. Diamond, J. Huang, The ITZ in concrete–a different view based on image analysis and SEM observations, Cem. Concr. Compos. 23 (2) (2001) 179–188.
[5] Y. Gao, et al., Porosity characterization of ITZ in cementitious composites: concentric expansion and overflow criterion, Constr. Build. Mater. 38 (2013) 1051–1057.
[6] K.L. Scrivener, et al., The interfacial transition zone (ITZ) between cement paste and aggregate in concrete, Interface Science 12 (4) (2004) 411–421.
[7] P.E. Stutzman, Scanning Electron Microscopy in Concrete Petrography, 2 National Institute of Standards and Technology, 2001.
[8] V.W. Tam, et al., Microstructural analysis of recycled aggregate concrete produced from two-stage mixing approach, Cem. Concr. Res. 35 (6) (2005) 1195–1203.
[9] D.P. Bentz, Influence of silica fume on diffusivity in cement-based materials: II. Multi-scale modeling of concrete diffusivity, Cem. Concr. Res. 30 (7) (2000)

1121–1129.
[10] I.S. del Bosque, et al., Properties of interfacial transition zones (ITZs) in concrete containing recycled mixed aggregate, Cem. Concr. Compos. 81 (2017) 25–34.
[11] W. Li, et al., Interfacial transition zones in recycled aggregate concrete with different mixing approaches, Constr. Build. Mater. 35 (2012) 1045–1055.
[12] P. Mondal, Nanomechanical Properties of Cementitious Materials, Northwestern University, 2008.
[13] J.A. Rossignolo, et al., Improved interfacial transition zone between aggregate-cementitious matrix by addition sugarcane industrial ash, Cem. Concr. Compos. 80 (2017) 157–167.
[14] A.R. Sakulich, V.C. Li, Nanoscale characterization of engineered cementitious composites (ECC), Cem. Concr. Res. 41 (2) (2011) 169–175.
[15] L. Sorelli, et al., The nano-mechanical signature of ultra high performance concrete by statistical nanoindentation techniques, Cem. Concr. Res. 38 (12) (2008) 1447–1456.
[16] J. Xu, et al., Modification effects of nanosilica on the interfacial transition zone in concrete: a multiscale approach, Cem. Concr. Compos. 81 (2017) 1–10.
[17] Y. Li, et al., Study on adhesion between asphalt binders and aggregate minerals under ambient conditions using particle-modified atomic force microscope probes, Constr. Build. Mater. 101 (2015) 159–165.
[18] Y. Li, et al., Adhesion between modified binders and aggregate minerals at ambient conditions measured with particle-probe scanning force microscopes, J. Mater. Civ. Eng. 29 (8) (2017) 04017068.
[19] C. Meyer, The greening of the concrete industry, Cem. Concr. Compos. 31 (8) (2009) 601–605.
[20] T. Bakharev, Geopolymeric materials prepared using Class F fly ash and elevated temperature curing, Cem. Concr. Res. 35 (6) (2005) 1224–1232.
[21] P. Duxson, et al., Geopolymer technology: the current state of the art, J. Mater. Sci. 42 (9) (2007) 2917–2933.
[22] P. Duxson, et al., The role of inorganic polymer technology in the development of 'green concrete', Cem. Concr. Res. 37 (12) (2007) 1590–1597.
[23] J.L. Provis, et al., J. Geopolymer technology and the search for a low-CO_2 alternative to concrete, 2007 AIChE Annual Meeting, American Institute of Chemical Engineers Salt Lake City, UT, United States, 2007.
[24] B.V. Rangan, et al., Properties and applications of fly ash-based concrete, Materials Forum, 2006.
[25] M. Sofi, et al., Engineering properties of inorganic polymer concretes (IPCs), Cem. Concr. Res. 37 (2) (2007) 251–257.
[26] I. Garcia-Lodeiro, et al., Compatibility studies between NASH and CASH gels. Study in the ternary diagram Na_2O–CaO–Al_2O_3–SiO_2–H_2O, Cem. Concr. Res. 41 (9) (2011) 923–931.
[27] J. Němeček, et al., Nanoindentation characteristics of alkali-activated aluminosilicate materials, Cem. Concr. Compos. 33 (2) (2011) 163–170.
[28] V. Šmilauer, et al., Application of micromechanics on alkali-activated materials, Advances in Science and Technology, Trans Tech Publ., 2010.
[29] P.G. Allison, et al., Nanoindentation and SEM/EDX characterization of the geopolymer-to-steel interfacial transition zone for a reactive porcelain enamel coating, Compos. Part B 78 (2015) 131–137.
[30] W. Lee, J. Van Deventer, The interface between natural siliceous aggregates and geopolymers, Cem. Concr. Res. 34 (2) (2004) 195–206.
[31] M. Miller, et al., Surface roughness criteria for cement paste nanoindentation, Cem. Concr. Res. 38 (4) (2008) 467–476.
[32] K. Kjellsen, et al., Preparation of flat-polished specimens for SEM-backscattered electron imaging and X-ray microanalysis—importance of epoxy impregnation, Cem. Concr. Res. 33 (4) (2003) 611–616.
[33] A. Onuma, et al., Quantitative analysis of nanoscale step dynamics in high-temperature solution-grown single crystal 4H-SiC via in situ confocal laser scanning microscope, Cryst. Growth Des. 17 (5) (2017) 2844–2851.
[34] J. Sandak, C. Tanaka, Evaluation of surface smoothness by laser displacement sensor 1: effect of wood species, J. Wood Sci. 49 (4) (2003) 305–311.
[35] M.K. YAMADA, F. WATARI, Imaging and non-contact profile analysis of Nd: YAG laser-irradiated teeth by scanning electron microscopy and confocal laser scanning microscopy, Dent. Mater. J. 22 (4) (2003) 556–568.
[36] Y. Zou, et al., A method for multi-resolution characterization on porous surfaces by using a laser confocal scanning microscope, Opt. Lasers Eng. 74 (2015) 40–46.
[37] H.N. Walker, Petrographic Methods of Examining Hardened Concrete: A Petrographic Manual, (1997).
[38] J. Xiao, et al., Properties of interfacial transition zones in recycled aggregate concrete tested by nanoindentation, Cem. Concr. Compos. 37 (2013) 276–292.
[39] J. Němeček, Creep effects in nanoindentation of hydrated phases of cement pastes, Mater. Charact. 60 (9) (2009) 1028–1034.
[40] C. Pichler, R. Lackner, Upscaling of viscoelastic properties of highly-filled composites: investigation of matrix–inclusion-type morphologies with power-law viscoelastic material response, Compos. Sci. Technol. 69 (14) (2009) 2410–2420.
[41] W.C. Oliver, G.M. Pharr, An improved technique for determining hardness and elastic modulus using load and displacement sensing indentation experiments, J. Mater. Res. 7 (6) (1992) 1564–1583.
[42] A. Elsharief, et al., Influence of aggregate size, water cement ratio and age on the microstructure of the interfacial transition zone, Cem. Concr. Res. 33 (11) (2003) 1837–1849.
[43] J. Maso, Interfacial Transition Zone in Concrete, 11 CRC Press, 2004.
[44] K.L. Scrivener, et al., Quantitative characterization of the transition zone in high strength concretes, Adv. Cem. Res. 1 (4) (1988) 230–237.
[45] W.A. Tasong, et al., Aggregate-cement paste interface: part I. Influence of aggregate geochemistry, Cem. Concr. Res. 29 (7) (1999) 1019–1025.
[46] J. Grandet, J. Ollivier, New method for the study of cement-aggregate interfaces, Proc. 7th International Congress on the Chemistry of Cement, Paris, 1980.